Int. J. Electrochem. Sci., 17 **(2022)** Article Number: 221275, doi: 10.20964/2022.12.75

International Journal of
ELECTROCHEMICAL
SCIENCE
www.electrochemsci.org

Individual and Simultaneous Electrochemical Determination of Vanillin and Caffeine Using Nafion/Ethylenediamine Grafted Multi-walled Carbon Nanotubes Modified Boron-doped Diamond Electrode

Babak Hatami Baroogh[1], *Asiye Aslıhan Avan*[2], *Hayati Filik*[2,*], *Sibel Yalçın*[2]

[1] Istanbul University-Cerrahpaşa, Department of Chemistry, Institute of Graduate Studies, 34320 Avcılar, Istanbul, Turkey
[2] Istanbul University-Cerrahpaşa, Faculty of Engineering, Department of Chemistry, 34320 Avcılar, Istanbul, Turkey
[*]E–mail: filik@istanbul.edu.tr

Received: 6 October 2022 / *Accepted:* 19 November 2022 / *Published:* 27 December 2022

A boron-doped diamond electrode (BDDE) modified with Nafion-ethylenediamine grafted multiwalled carbon nanotubes (EDA-MWCNTs) composite was fabricated for the simultaneous quantification of Vanillin (VAN) and Caffeine (CAF). Firstly, the MWNTs are functionalized with acyl chloride groups, which further react with EDA to form amine-functionalized MWCNTs. The experimental findings showed that the modified BDDE had high activity for the electrochemical oxidation of both compounds. In 0.10 M H_2SO_4, the linear range for the detection of binary mixtures of VAN and CAF with square wave voltammetry (SWV) was 0.4-40 µM and the reached detection limits were 0.15 µM and 0.18 µM (LOD =3SD/m), respectively. The modified BDDE was successfully utilized to establish VAN and CAF in different samples with recoveries range of 94%−102% and 95%−100%, respectively.

Keywords: Vanillin, Caffeine, boron-doped diamond electrode, ethylenediamine, multi-walled carbon nanotubes, electrochemical sensor

1. INTRODUCTION

Vanilla (*Vanilla planifolia A*) is the most popular flavour. It is used broadly in the current industries, including the pharmaceutical, cosmetic, tobacco, food, and beverage industries. Vanillin (4–hydroxy–3–methoxy benzaldehyde) is the primary ingredient of vanilla of pure vanilla extract [1]. Natural vanillin is generally provided from the orchid Vanilla planifolia and its bean [2]. Only a small quantity of vanillin utilized in beverages and foods is extracted from the plant due to its high cost. Most of the vanillin was gained through chemical synthesis or biotechnological fabrication [3] and synthetic

vanillin was generally used for the production of numberless household products, air fresheners, deodorants, floor polishes, herbicides and so on [3,4]. According to the limitations of the FDA, the quantity of vanillin in food should not exceed 70 mg kg^{-1}. Caffeine (1,3,7-trimethylxanthine) (CAF) is a purine alkaloid which varies in the number and position of the methyl substituent in the xanthine ring i.e., 1,3,7- trimethyl xanthine [5]. CAF is a mild stimulant and the most routinely used drug in the world. It is found in many foods and drinks (coffee and tea). CAF can cause adverse reactions such as nervousness, insomnia, nausea, gastrointestinal problem, restlessness, elevated heart rate, and other side effects. However, the surplus intake of CAF may cause tachycardia and tremor to a larger extent and eventually drive to death [6,7]. Consequently, individual or simultaneously determining the concentrations of both molecules is needed not only for quality control but also to investigate the influences of these molecules on the human body.

To date, both analytes have been determined via many techniques, such as high-performance liquid chromatography (HPLC), gas chromatography/mass spectrometry (GC/MS), capillary electrophoresis (CE), and UV–vis spectroscopy [8–10]. The above-mentioned analytical methods can accurately separate and determine VAN and CAF content. Compared to electroanalytical protocol, other methods (HPLC, GC-MS, CE, and UV-vis) require costly equipment, a versatile laboratory environment, complex and time-consuming processes, and an accomplished user for efficient operation. Due to the advantages of low cost, ease to use, and fast results of electrochemical approaches, electrochemical-based sensors have been intended and developed for the sensing of VAN and CAF. In the literature, a large number of types of modified electrodes have been informed recently for the individual (along) sensing of VAN [11–16] and CAF [17–21]. VAN and CAF are two added ingredients and commonly coexist in many food products. Their simultaneous assessment of food products is, therefore, a considerable task. However, to date, a very limited number of electrochemical-based methods have been reported for the simultaneous assessment of both molecules. For example, Jiang et al. [22] synthesized nitrogen-doped graphene/carbon nanotubes (NGR–NCNTs) and the electrochemical success of the bare GCE modified with electrodeposited NGR–NCNTs towards VAN and CAF sensing was proved by CV and SWV. Poly(alizarin red S) conducting polymer was attached to the bare GCE surfaces, and the poly(alizarin red S)/GCE was successfully used for the simultaneous sensing of both target analytes [23]. The BDDE*s* were effective sensors for the trace detection of organic molecules in an aqueous solution. In this regard, Ali et al. [24] reported a voltammetric procedure for the simultaneous prediction of VAN and CAF utilizing an anodically pretreated BDDE (APT-BDDE). Similarly, the voltammetric efficiency of APT-BDDE and cathodically pretreated BBDE (CPT-BDDE) in the oxidation of a ternary mixture of 5-O-caffeoylquinic acid (5-CQA), VAN and CAF were properly tested by carrying out stripping voltammetric measurements [25]. Further study on the simultaneous evaluation of VAN and CAF was realized at the complex-modified GCE. In this work, the working electrode was constructed by electropolymerized aniline (PANI) on MoS_2/graphitic carbon nitride (g-C_3N_4) modified GCE (MoS_2/PANI@g-C_3N_4/GCE). The sensor was employed for simultaneous quantification of VAN, theophylline (TP), and CAF with high oxidation peaks and well-defined voltammetric responses, using DPV measurements [26]. Alternatively, MoS_2/PANI/f-MWCNTs ternary hybride architecture was prepared through a simple conventional technique and covered on a GCE surface to create MoS_2/PANI/f-MWCNTs modified GCE and the invented sensor was applied for

simultaneous sensing of VAN, CAF, and theophylline (TP) in food and beverage samples, The detection limit of the sensor was equal to 0.021, 0.051, and 0.042 μM for VAN, CAF, and TP, respectively [27]. An electrochemical sensor based on the electrocatalytic activity of graphene (GR) was developed and employed for the individual and simultaneous detection and quantification of 5-*O*-Caffeoylquinic acid (5-CQA), VAN and CAF. The important analytical criteria of three target analytes on GR-modified GCE were examined by square-wave adsorptive stripping voltammetry. This GR-based device exhibited 4.4×10^{-9}, 5.0×10^{-7}, and 3.0×10^{-7} M limit of detection for 5-CQA, VAN and CAF, respectively [28]. In recent days, the WS_2/chitin/polypyrrole (PPy) hybride was synthesized for a paper-type self-powered multifunctional electrochemical device integrated energy-storage system. The above-mentioned hybrides were performed as a sensor (or supercapacitor) for the simultaneous sensing of VAN and CAF. The WS_2/chitin/PPy hybride modified paper device exhibited a specific capacitance of 381.5 Fg^{-1} for O-chitin and 311.3Fg^{-1} for C-chitin based composites and their corresponding sensitivity performances were also good for both VAN and CAF detection experiments [29].

Implementations of the BDDE-based sensors in the electrochemical assay of organic compounds have also been explored recently [26,30–32]. High stability, the low adsorption of organic molecules on the electrode surface, wide potential window and low background current have been claimed as technologically important properties that differentiate the BDD from traditional working electrodes such as GC and highly oriented pyrolytic graphite (HOPG). BDDEs can be useful for the sensitive detection of various substances, including organic pollutants. drugs, bio-related substances, and heavy metal ions. The electrochemical active surface area of BDDEs is heterogeneous and therefore, electron transfer at the heterogeneous surface of BDD is inhibited for many redox reactions. However, the electrochemical interaction of many reactive species on BDDEs can be enormously hanging on whether their characteristics are especially hydrogen-terminated (HT) and oxygen-terminated (OT). The CPT-BDDE is rich in HT while APT-BDDE is rich in OT. Especially, the HT and OT diamonds have displayed different surface behaviors, such as surface conductivity, electron affinity, and work function. Thus, when convenient, the surface activity of a BDDE for a target analyte may be regulated by electrochemical pretreatments, yielding improved sensing features [24,25,33–35]. On the other hand, surface modification of the BDDEs using nanocarbon materials, metal nanoparticles, and polymers can improve the sensitivity of electrochemical detection [30–32,36]. The common approaches towards the attachment of such materials onto BDDEs include electrochemical polymerization, electrochemical deposition, photochemical reaction, and ion implantation. The relatively simple technique of drop-casting a coating onto BDDE is rather limited [37].

In the present work, Nafion-EDA-MWCNTs modified BDDEs were constructed by a simple and rapid drop-casting process. Nafion-EDA-MWCNT nanomaterials-based sensors have been fabricated for simultaneous voltammetric sensing of VAN and CAF with high sensitivity making them appropriate for encouraging implementations in aqueous samples. There is no report based on using Nafion-EDA-MWCNTs modified BDDE for the simultaneous sensing of VAN and CAF.

2. EXPERIMENTAL

2.1. Chemicals and solutions

VAN (99%, ReagentPlus®), CAF (99%), Ethylenediamine (EDA) (liquid, 99%), Nafion™ (5 wt%), Trichloroacetic acid (TCA), H_2SO_4 (96%), KCl and Multi-walled carbon nanotube (MWCNTs, >95% carbon basis, diameter: 10-20 nm, length: 20-50 μm) were purchased from Sigma-Aldrich (USA). $SOCl_2$ (purity:99%, density: 1.638 g/cm^3, liquid), tetrahydrofuran (THF), HNO_3, (70%), $K_4[Fe(CN)_6].3H_2O$, and $K_3[Fe(CN)_6]$ were purchased from Merck. Theophylline (Thb) and theobromine (Thp) have been bought from Fluka and Sigma–Aldrich. Stock solutions of VAN (2×10^{-3} M) and CAF (2×10^{-3} M) were properly prepared with an ethanol/water mixture (1:4 v/v), respectively. The stock solutions were stored in a refrigerator (4 °C) when not in use. Solutions with a concentration of 0.4-40 μM VAN and CAF were prepared as calibration standard working solutions by dilution of stock solution with a mixture of ethanol/water (1:4 v/v). All chemicals were used as received without further purification. All solutions are prepared on the day of the experiments.

2.2. Instruments

The electrochemical measurements (CV, EIS, and SWV) were made with Gamry series 600 potentiostat/galvanostat. All measurements were recorded using a 10 mL electrochemical cell that has a three-electrode system. The following electrodes are employed in a three-electrode setup: The bare or modified BDDE, Ag/AgCl (3 M KCl), and platinum wire were employed as working electrodes, a reference and counter electrodes, respectively. The BDDE surface was carefully shined mechanically daily with the use of alumina slurry (0.3 μm, Buehler) on the shining pad (Buehler) and after rinsing in distilled water. Fourier transform infrared spectrum (FTIR) measurements were actualized using a Bruker Tensor 27 (Bruker Optics, Ettlingen, Germany). Raman spectra were recorded on a Renishaw in Via Raman Microscope (UK). The surface morphology of nanomaterial was examined by using a scanning electron microscope (SEM) (ZEISS Merlin FE SEM, Germany), and transmission electron microscopy (TEM) (FEI TALOS F200S TEM, USA).

2.3. Synthesis of Nafion-EDA-MWCNTs

Synthesis of oxidized MWCNTs (ox-MWCNTs): 0.1 g of MWCNTs were treated at 40 °C with 25 mL of a mixture of H_2SO_4 (96%)/HNO_3 (70%) (3/1), in a flask connected to a condenser for 6h. Subsequently, the resulting mixture was diluted (9:1) in distilled water and filtered. Then, the products (ox-MWCNTs) were appropriately washed with distilled water several times until neutral pH was reached and the products were dried in a vacuum oven (10-25 millibar) at 50 °C overnight. Furthermore, the ox-MWCNTs (~ 0.1 g) were treated with excess neat $SOCl_2$ (99%, 25 mL, 0.342 mol) for 24 h under reflux (the reaction temperature was 65-70 °C). After that, the excess $SOCl_2$ was eliminated by the distillation process and the product (MWCNT-COCl) was properly washed with THF and then filtered using cellulose filter papers. The obtained solid MWCNT-COCl (~ 0.1 g) was placed in a 25 mL round

bottom flask, and 10 mL of EDA was added and stirred under ultrasonication for 2 h until the uniform suspension was obtained. The MWCNT-COCl was immediately reacted with liquid EDA for 48 h at 100 °C. The reaction mixture was cooled to ambient temperature and washed with ethanol to remove the excess EDA, and then dried in an oven at 50 °C overnight. The resulting products (EDA-MWCNTs) were dispersed in a 10 mL (0.5 mg/mL) ethanol/water (1:1) mixture [38,39]. Furthermore, the preparation of Nafion-EDA-MWCNTs was based on the previous approaches [40]. In brief, the above-mentioned solution (10 mL) was ultrasonicated for 5 min at ambient temperature and subsequently, 0.1 mL of 5% Nafion (w/v) solution was introduced to the EDA-MWCNTs suspension and the corresponding mixture was ultrasonicated (20–40 kHz) at 50 °C for 30 min. The resulting architectures were named as Nafion-EDA-MWCNTs [40].

2.4. Electrode modification

Before alteration of the BDDE, its surface was properly shined with 0.05 μm alumina slurry and then washed with excess distilled water. The BDDE was then put under sonication to remove impurities on the surface of the BDDE and dried at room temperature. Modified electrodes were prepared by drop-casting modifier suspension (5 μL Nafion-EDA-MWCNTs) onto the active surface area of BDDE. The remaining solvent was then properly vaporized at room temperature to achieve Nafion-EDA-MWCNTs modified BDDE.

2.5. Sample Preparation

Samples of commercially-available vanilla sugar, energy drink, vanilla coffee, and iced tea were provided from a local market and assayed immediately after opening. For this, a 0.1 g of the homogenized powdered vanilla sugar from each brand was transferred to a 100 mL volumetric flask, dissolved with distilled water by sonication and the mixture solution was filtered by a syringe filter (GF/PET-1.0/0.45 μm) and finally, the volume was completed to the mark (100 mL) with distilled water. The energy drink and ice tea samples (each 25 mL) were degassed via sonication, filtrated by a syringe filter and then, distilled water was added to the final volume of 100 mL. Vanilla coffee*:* To precipitate the proteins (to prevent electrode passivation), a 10 mL milk sample was mixed with 0.4 mL TCA (Trichloroacetic acid) in a test tube and left on ice for 30 minutes. Then, the solid-liquid mixture was centrifuged at 5000 rpm for 5 min. The supernatant was systematically filtered and sufficient distilled water was added to make 20 mL and stored at 5°C.

3. RESULTS AND DISCUSSION

3.1. Electrochemical behavior of VAN and CAF

The voltammetric performance of the two analytes is studied by CV with BDDE (a), MWCNTs/BDDE (b), EDA-MWCNTs/BDDE (c) and Nafion-EDA-MWCNTs/BDDE (d), respectively,

in 0.1 M H_2SO_4 solution (the applied scan rate was 50 mV s^{-1}). As displayed in Fig. 1, when the concentrations of VAN and CAF are all 0.1 mM, two legible peaks can be obtained for the Nafion-EDA-MWCNTs/BDDE. Compared to those of the BDDE (a), MWCNTs/BDDE (b), and EDA-MWCNTs/BDDE (c) the peaks of VAN and CAF in the Nafion-EDA-MWCNTs/BDDE is increased. This circumstance may be because the electrochemical performance is increased by the synergistic action of the Nafion-EDA MWCNT nanostructures (excellent electrocatalytic activity). The comprehensible peaks of VAN and CAF (0.905 V and 1.359 V, respectively) further demonstrate that the Nafion-EDA-MWCNTs modified BDDE exposes better catalytic activity for their simultaneous and selective quantification.

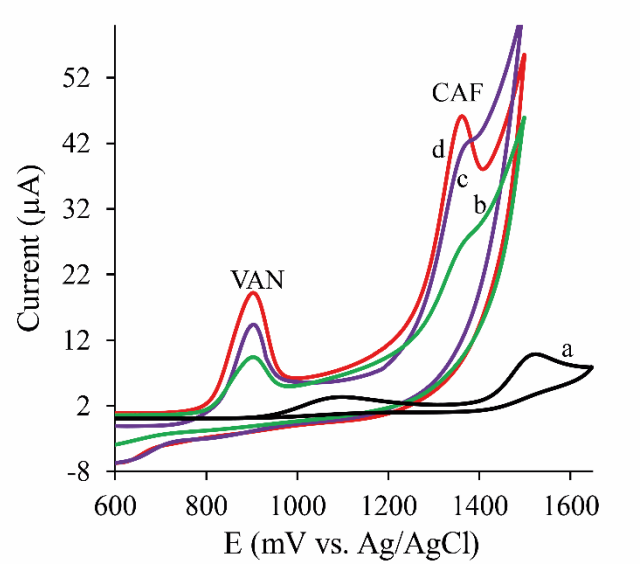

Figure 1. CV curves of VAN and CAF (a binary mixture, each 0.1 mM) on different electrodes bare BDDE (a), MWCNTs/BDDE (b) EDA-MWCNTs/BDDE (c) Nafion-EDA-MWCNTs/BDDE (d) supporting electrolyte: 0.10 M H_2SO_4, scan rates: 50 mV s^{-1}.

3.2. Effect of scan rate

The scan rate dependency of CV for the Nafion-EDA-MWCNTs/BDDE experimented in the 0.1 M H_2SO_4 containing 0.1mM VAN and 0.1 mM CAF. It can be found from the result in Fig. 2 that the anodic peak potentials shift slightly to a more positive direction with the increase in voltage scan rate. In the meantime, the anodic peaks of two analytes at the Nafion-EDA-MWCNTs/BDDE increase linearly with the voltage scan rate in the range of 10-500 mV/s. It can result that the anodic peak potentials were dependent on the scan rate. The following regression equations of both analytes can be derived from Fig. 2.

$I\ (\mu A) = 0.2521\ \nu\ (mV/s) + 4.242\ (R^2 = 0.9962)$ for VAN

$I\ (\mu A) = 0.2354\ \nu\ (mV/s) + 0.025\ (R^2 = 0.9984)$ for CAF

On the other hand, for the plot of I_{pa} vs. log υ, the regression equations are derived as:

$\log I\ (\mu A) = 0.8643 \log \nu\ (mV/s) - 0.233\ (R^2 = 0.9984)$ for VAN

$\log I\ (\mu A) = 0.9508 \log \nu\ (mV/s) - 0.517\ (R^2 = 0.9925)$ for CAF

The slope value obtained from the two graphs (Fig. 2B) was 0.864 for VAN and 0.951 for CAF and it is near to the theoretical value for the adsorption-controlled process. Furthermore, the standard heterogeneous rate constant (k^0) can be calculated by the Laviron equation (Eq 1) [41]:

$$E_{pa} = [2.303RT/(1 - \alpha)n\alpha F)]\log v + K \quad (1)$$

According to the linear correlation between Epa and ln*v*, the slope is equal to ~ *E*pa =RT/*α*nF (Eq 1) where E_{pa} is the formal redox potential of the analyte, *R* is (*R* = 8.314) the universal gas constant, *T* is the absolute temperature (298°K), *α* is the electron transfer coefficient of the analyte, *F* is Faradays constant (96485). The '*αn*' value has been derived from the slope of E_p *vs* log ν. Based on the findings, we can also obtain the regression equations.

E_{pa} (V) = 0.0251 ln*v* (mV/s) + 0.790 (R^2 = 0.9976) for VAN

E_{pa} (V) = 0.0132 ln*v* (mV/s) + 1.307 (R^2 = 0.9966) for CAF

In this experiment, the slope value was calculated to be 0.0251 for VAN and 0.0132 for CAF. For an irreversible voltammetric process, α value can be utilized as 0.5. Therefore, the number of electrons involved in the electro-oxidation reaction was 2 for VAN and 4 for CAF. In addition, the intercept of the E_p vs ln ν curve was 0.7899 for VAN and 1.3067 for CAF. Hence, the value of k° was found to be 18 μs^{-1} and 30 μs^{-1}, respectively. In light of these findings, Nafion-EDA-MWCNTs/BDDE provided the largest active surface area, resulting in the highest sensitivity.

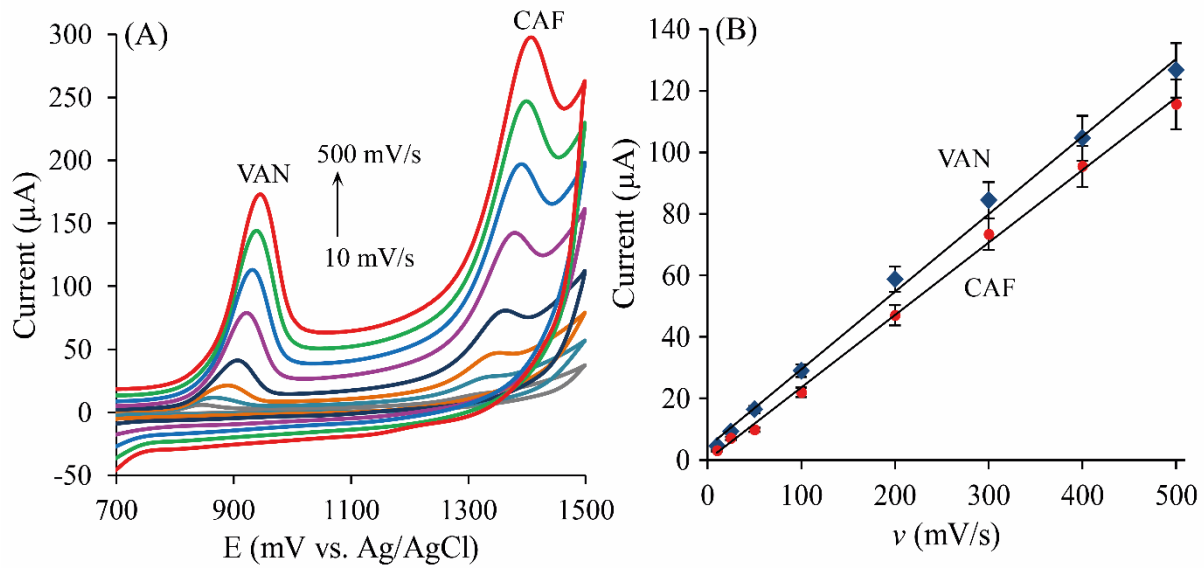

Figure 2. (A) CV profiles of VAN and CAF (a binary mixture, each 0.1 mM) in 0.1 M H_2SO_4 at a scan rate of 10, 25, 50, 100, 200, 300, 400 and 500 mV s^{-1}. (B) The relationship between the peak currents and the scan rates.

3.3. EIS and CV analysis

During the step-by-step modification process, the EIS is a crucial technique to qualify the electron transfer attributes of the surface of the electrode. Fig. 3A shows the EIS of different electrode surfaces BDDE (a), Nafion/BDDE (b) EDA-MWCNTs/BDDE (b) Nafion-EDA-MWCNTs/BDDE (c) in 0.1 M KCl containing 5.0 mM $[Fe(CN)_6]^{3-/4-}$. Initially, the charge transfer resistance (R_{ct}) value for

the bare BDDE measured was 876 Ω (Fig. 3A, curve a). Furthermore, the R_{ct} of Nafion/BDDE (b), EDA-MWCNTs/BDDE (c), and Nafion-EDA-MWCNTs/BDDE (d) obtained were 382 Ω, 22 Ω, and 16 Ω, respectively. When the BDDE was modified with MWCNTs (curve b) and EDA-MWCNTs (curve c), and Nafion-EDA-MWCNTs/BDDE, the diameter of the semicircle for the modified electrode diminished markedly and R_{ct} decreased greatly, to 16 Ω. Through the comparison of the four EIS profiles, it can be displayed that the semicircle diameter of EIS plots progressively reduces representing the Nafion-EDA-MWCNTs composite with high catalytic activity and seriously streamlined the electron transfer of $[Fe(CN)_6]^{3-/4-}$ probe on the working electrode surface, and consequently, decreased surface diffusion capacitance and R_{ct} value. Therefore, the EDA-MWCNTs are convenient for electrochemical sensing. In this system, the Nafion plays a key role in preparing a homogeneous and well-distributed EDA-MWCNT film. The results showed that the Nafion-EDA-MWCNT/BDDE was successfully prepared by this route.

CV curves of BDDE, Nafion/BDDE (b), EDA-MWCNTs/BDDE (c), and Nafion-EDA-MWCNTs/BDDE (d) were tested in 0.1 M KCl solution containing 3.0 mM $[Fe(CN)_6]^{3-/4-}$ at the scan rate of 50 mV s^{-1} (Fig. 3B). It can be noticed that CV shows a good reversible wave, which is caused by the redox reaction of ferricyanide on the electrode surface. The peak value of the EDA-MWCNTs/BDDE (c) is significantly increased compared with that of BDDE (a) (34 µA), Nafion (b) (42 µA), and EDA-MWCNTs (c) (63 µA).

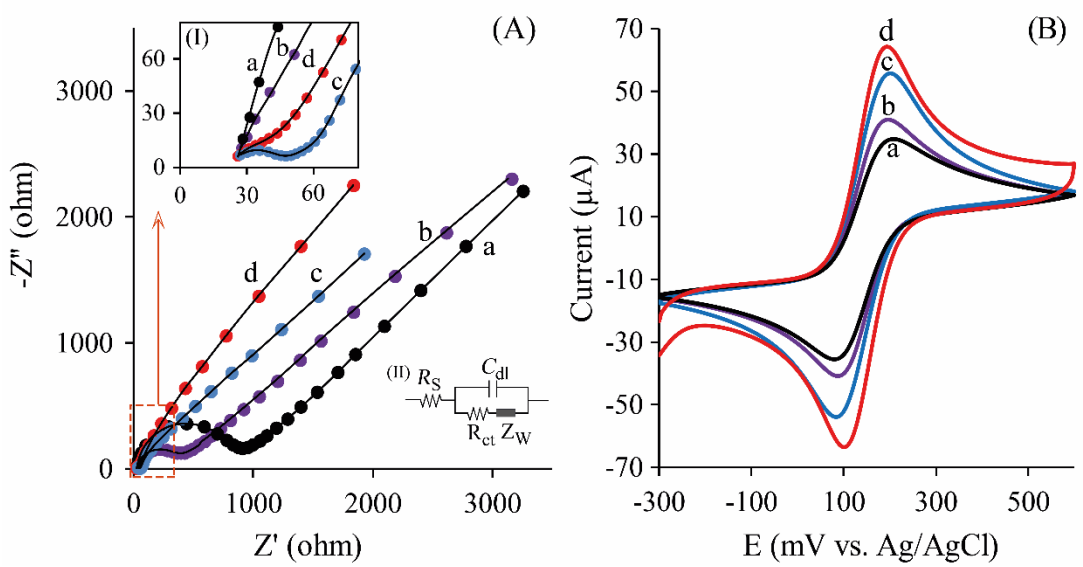

Figure 3. (A) EIS patterns of bare BDDE (a), Nafion/BDDE (b), EDA-MWCNTs/BDDE (c) Nafion-EDA-MWCNTs/BDDE (d) in a solution containing 5.0 mM $Fe(CN)_6^{3-/4}$ (1:1, v/v) and 0.1 M KCl, the frequency range is 0.1 Hz-100 kHz, and the amplitude is 10 mV. The insert in (I) shows the EIS spectra in the higher frequency interval. The insert in (II) displays an equivalent circuit model applied to fit the Nyquist plots. R_S, electrolyte solution resistance; C_{dl}, double layer capacitance of the electrode; R_{ct}, charge transfer resistance; Z_W, Warburg impedance resulting from the diffusion of ions; Nyquist plot of experimental (colored symbols) and fitted results (lines). (B) CV profiles of bare BDDE (a), Nafion/BDDE (b) EDA-MWCNTs/BDDE (c), Nafion-EDA-MWCNTs/BDDE (d) in 0.1 mol/L KCl containing 3.0 mM $Fe(CN)_6^{3-/4-}$.

The potential difference between two peaks ($\triangle E_p = E_{pa}$-E_{pc}) of the Nafion-EDA-MWCNTs (d) was calculated to be 93.5 mV, which is smaller than that of other test materials, indicating Nafion-EDA-MWCNTs shows better electrochemical performance. Moreover, the peak current of the Nafion-EDA-MWCNTs (63 μA) is the highest among all electrode materials. Thus, Nafion exhibits both ionic and hydrophobic interactions with the BDDE surface to form a stable layer [42–44].

For reversible CV reactions, the peak current can be used to calculate the active surface area of the modified electrode on basis of the Randles-Sevcik formula.

$$I_p=2.69 \times 10^5 A(D.v)^{1/2} n^{3/2} C \quad (2)$$

Where *Ip, A, D, n, v,* and *C* symbolize the peak current, the surface area (cm^2), the diffusion coefficient ($D = 6.67 \times 10^{-6}$ cm^2 s^{-1}), the number of electrons (n = 1), the scanning rate (v = 0.050 V s^{-1}), the concentration of $[Fe(CN)_6]^{3-/4-}$ (C = 5.0 mM), respectively. Compared with other modified electrodes (Nafion, 0.09 cm^2 and EDA-MWCNTs, 0.12 cm^2), Nafion-EDA-MWCNT/BDDE has a higher electroactive surface area (0.14 cm^2), showing that Nafion-EDA-MWCNTs has good conductivity, which promotes the electron transfer of ferricyanide ion on the electrode surface, speeding up the reaction.

3.4. Surface characterization

3.4.1. FTIR and Raman analysis

To estimate how EDA molecules attach to the MWCNT-CO-Cl surface, FTIR analysis was employed for the MWCNTs, ox-MWCNTs, and EDA grafted MWCNTs, respectively, and the FTIR spectra obtained are illustrated in Fig. 4A. The FTIR spectrum of the MWCNTs displayed the weak stretching vibrations (symmetric and asymmetric) of the –CH groups at 2950–2800 cm^{-1} zone, and a strong and broad peak characteristic of the O–H group vibrations at ∼3410 cm^{-1} are monitored. For the ox-MWCNTs without EDA modification (Fig. 4A, curve a), in particular, the oxygen-rich groups give rise to a C–O stretching peak at ∼1168 cm^{-1} and a carboxyl peak at ∼1712 cm^{-1} [45,46]. Furthermore, the stretching vibration intensity of the -OH group is improved remarkably. From the FTIR spectrum of the EDA-grafted MWCNTs (curve b in Fig. 4A), several extra adsorption peaks can be monitored. In this regard, the FTIR spectrum for EDA-MWCNTs displays peaks at 1748 cm^{-1} (C=O stretching), 1520 cm^{-1} (C–C stretching), 1455 (C–H stretching), 1293 cm^{-1}(C–N stretching) and 1063 cm^{-1} (C–O stretching) for ox-MWCNTs is a clear indication of the interactions of EDA with MWCNTs via –CO-Cl groups to form amide linkages to form –OH and –NHR groups [45,46]. The FTIR profile assignments verify that the MWCNTs had been adequately oxidized into the shorter carboxylated MWCNTs (MWCNTs-COOH) and after which, EDA molecules were properly introduced into the MWCNTs-COOH. Based on the above findings, the EDA molecules were successfully attached to the MWCNTs surface or -COOH (-CO-Cl) groups.

It has been observed that the defect-rich carbon architectures facilitate the formation of catalytic sites for enhancing electrochemical activity. Raman spectral analysis permits the evaluation of the irregularity and defects in carbon architectures through the measurement of the peak ratio ((I_D/I_G) ratio) of the D band to the G band. Raman spectral analysis is depicted in Fig. 4B. The characteristic peaks of

graphite materials with a D-band peak located at 1336 cm^{-1} are identified, which are related to defects. The G peak was monitored at 1576 cm^{-1} while the G peak arises from the graphite peak corresponding to the behavior in contrary directions of the C–C bonds in MWCNTs. In brief, the characteristic mode peaks for MWCNTs were located at 1336 cm^{-1} for the disorder mode peak and 1576 cm^{-1} tangential mode peak. Based on Fig. 4B, the calculated I_D/I_G ratio was 0.84. When the EDA molecule is attached to the surface of MWCNTs via a covalent bond, real sp^2 carbon is changed to sp^3 carbon [47]. In this case, the proportion of sp^2 decreases while sp^3 carbon increases in quantity, which would result in I_D/I_G ratio (0.82) reduced. As a result, the I_D/I_G ratio of the MWCNT-carboxyl was 0.84, which was higher than that of MWCNTs functionalized by the EDA molecule. The findings indicated that the content of sp^3 hybridization improved resulting from the interactions between the active carboxyl group on the surface of MWCNTs and the active amino group that collapsed the order mode of the MWCNTs.

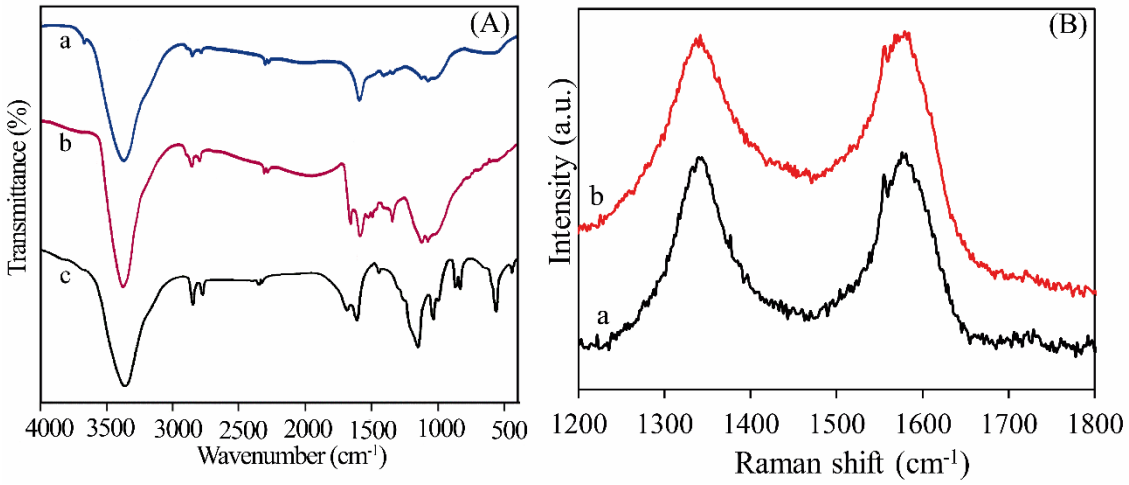

Figure 4. (A) The FTIR spectra of the pristine MWCNTs (a), MWCNTs–COOH (b), and MWCNTs–$CONH_2$ (c), Raman spectra of MWCNTs-COOH (a), EDA-MWCNTs (b).

3.4.2. SEM and TEM analysis

The surface morphologies of MWCNTs-COOH (a) and MWCNTs–COEDA (or MWCNTs–$CONH_2$) nanocomposite (b) were photographed using SEM as shown in Fig. 5 (A and B). The morphology of the MWCNTs-COOH surface did not change considerably after EDA modification (EDA-MWCNTs), as observed by SEM images (Fig 5 A and B).

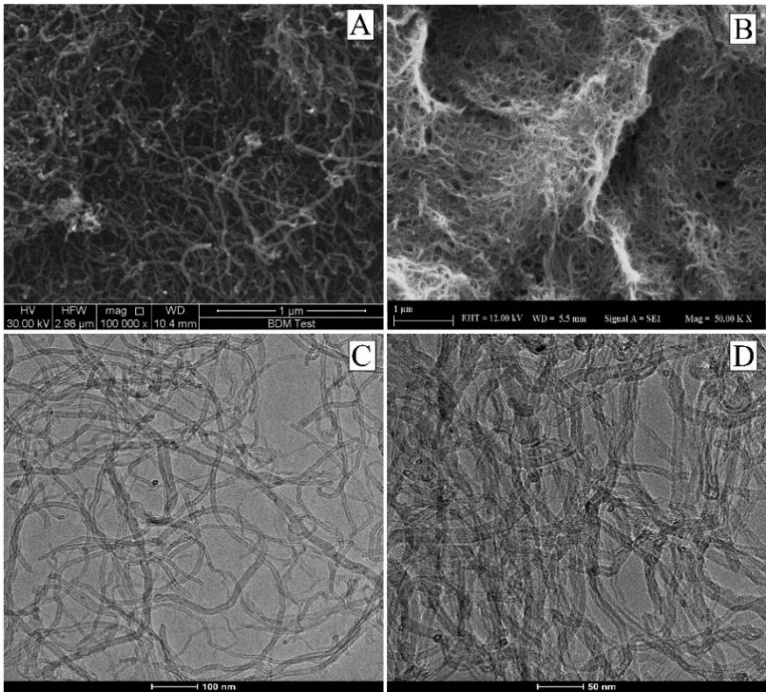

Figure 5. SEM (A and B) and TEM (C and D) images of MWCNTs-COOH and EDA-MWCNTs, respectively.

After grafting of MWCNTs using EDA, the SEM images of EDA-MWCNTs show a uniform distribution of long and hollow MWCNTs along with successful grafted with EDA and the morphology of the EDA-MWCNTs were observed as multi-stacked layers. On the other hand, EDA-MWCNTs display clear visualization due to the complete removal of the reaction product as a result of effective functionalization.

To receive further insight into the agglomeration of ox-MWCNTs after modification by EDA, the surface microstructures of the grafted composites were observed using TEM. In this case, the low magnification TEM profiles of ox-MWCNT and EDA-MWCNTs were recorded. A comparison of Fig. 5C and Fig. 5D displays that EDA-MWCNTs are more entwined than ox-MWCNTs, as defined by the absorbance of the corresponding suspensions. However, the agglomeration incited by the attachment of EDA on ox-MWCNTs surface is not intense, thus EDA-MWCNTs can probably be employed as electrochemical catalyst support.

3.5. Effect of H_2SO_4 concentrations

The best analytical results are obtained by the H_2SO_4 solution. The CVs of the Nafion-EDA-MWCNTs/BDDE in the solution comprising VAN and CAF (each 0.1 mM) at different H_2SO_4 concentrations are exhibited in Fig. 6. It declares that with an increase in H_2SO_4 concentration, the anodic peak potentials of both analytes shift negatively. Meanwhile, the peak current of VAN and CAF increases as the concentration of H_2SO_4 increases from 0.05 M to 0.1 M and subsequently, diminishes when the concentration of H_2SO_4 increases further. In this case, the best CV response reached 0.1 M H_2SO_4 (Fig. 6). Hence, 0.1 M H_2SO_4 was employed as the optimum for the simultaneous sensing of

VAN and CAF, and therefore, the mentioned H_2SO_4 concentration was chosen for the remaining electrochemical tests. Based on the above data, Fig. 6 displays the relation between H_2SO_4 concentration (from 0.05, 0.08, 0.1, 0.15 and 0.2 M) (pH value was 1.23, 1.04, 0.96, 0.79, and 0.67, respectively) and the peak potential (E_{pa}). The peak potentials of analytes shifted in the less negative direction with the increase of H_2SO_4 concentration, the findings define that the protons were directly involved in the electrochemical oxidation of VAN and CAF. However, the plot of anodic peak potential (E_{pa}) versus (pH) was also linearly expressed by the equations: E(V) = -0.0284 pH + 0.9345 (R^2 = 0.9973) for VAN and E(V)= -0.0306 pH + 1.3951 (R^2 = 0.9941) for CAF.

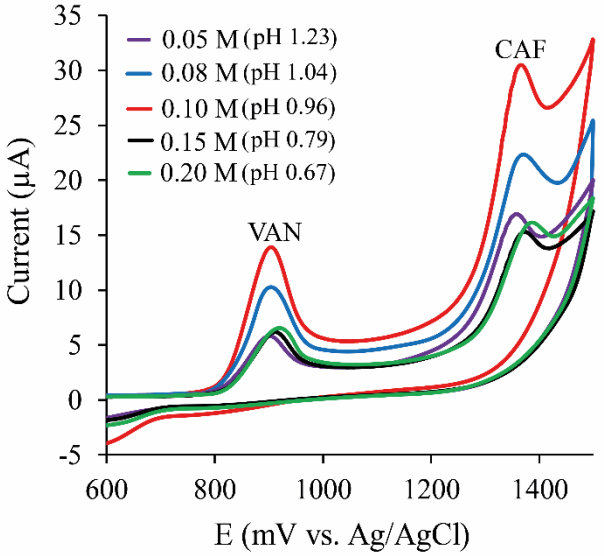

Figure 6. CV curves (scan rate 50 mV/s) of Nafion-EDA-MWCNTs/BDDE in the presence of CAF and VAN (a binary mixture, each 0.1 mM) at different concentrations of H_2SO_4 (0.05, 0.08,0.10, 0.15, and 0.2 M) and the solutions having pH values 1.23, 1.04, 0.96, 0.79, and 0.67, respectively.

3.6. Individual and simultaneous determination of VAN and CAF

The SWV technique was employed to show the sensing efficiency of the individual detection of two target analytes. Initially, SWV parameters such as frequency, step size, and pulse size for the simultaneous quantification of both targets in binary mixtures have been investigated and the achieved results were frequency 10 Hz, step size 8 mV, and pulse size 100 mV. In this respect, successive contrariwise binary mixtures have been prepared with one target at a constant concentration and the other target at differing concentrations. As depicted in Fig. 7, with increasing the concentration of VAN, the peak density increases linearly, while the peak density of 30 µM CAF nearly remained stable. The experimental findings indicated that the response current of VAN was directly proportional to the concentration in the range of 0.4 – 40 µM. The derived linear regression equation (LREq) was I(µA) = 1.9099 C_{VAN} (µM) + 0.7925 (R^2 = 0.9982). Fig. 7B indicates that the SWV response of CAF increases with increasing CAF concentration, while the peak density of 30 µM VAN nearly remained stable, as depicted in Fig. 7B. The response current of CAF was proportional to the concentration in the range of 0.4 – 80 µM. From the data, the linear regression equation was I(µA) = 1.507 C_{CAF} (µM) + 3.1155 (R^2 = 0.9952). The LOD was 0.12 µM for VAN and 0.17 µM for CAF (S/N = 3).

The main goal of this investigation was to develop a method for the simultaneous detection of VAN and CAF. For this reason, binary mixtures have been prepared from various equal concentrations of both analytes in the range 0.4-40 µM using 0.1 M H_2SO_4 and then, they have been assayed by the SWV technique, as illustrated in Fig. 7C. Effectively, the Nafion-EDA-MWCNTs modified BDDE has demonstrated an impressive independent efficiency in sensing each analyte in the binary mixture. According to the findings, the linear regression equation was I(µA) = 1.7252 C_{VAN} (µM) + 3.1028 (R^2 = 0.9968) for VAN and I(µA) = 1.507 C_{CAF} (µM) + 3.1155 (R^2 = 0.9952) for CAF. Additionally, the LODs of VAN and CAF were 0.15 µM and 0.18 µM, respectively. The LOD was calculated based on LOD=3SD/m [48]. In this equation, SD is the standard deviation of a concentration of 0.4 µM (binary solution, each 0.4 µM) measured with five replicates and m is the slope of the calibration plot.

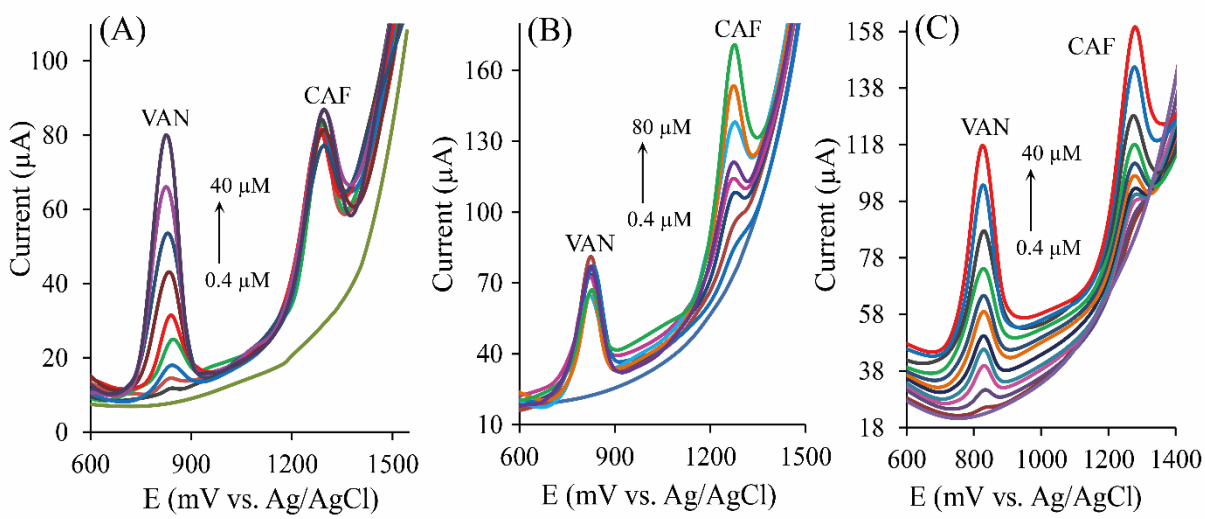

Figure 7. SWVs of Nafion-EDA-MWCNTs/BDDE with 30 µM CAF and various concentrations of VAN (0.4-40 µM) (A), 30 µM VAN and various concentrations of CAF (0.4-80 µM) (B) and various concentrations of CAF (0.4-40 µM) and VAN (0.4-40 µM) (C). Frequency 10 Hz, Step size 8 mV, Pulse size 100 mV.

3.7. Comparison of the method

The comparison of the analytical figure of the merits of the invented electrochemical sensor with previously declared sensors for simultaneous detection is shown in Table 1.

Table 1. Examples from the previously reported modified electrodes for simultaneous detection of VAN and CAF.

Modified electrode	Linear range (µM)		Detection Limit (µM)		Reference
	VAN	CAF	VAN	CAF	
NGR–NCNTs/GCE	0.01–10	0.06–50	0.0033	0.02	[22]
Poly(ARS)/GCE	10–450	0.5–250	0.06	0.8	[23]
APT-BDDE	6.6–660	5.2–520	1.54	0.37	[24]
CPT-BDDE	6.7–330	0.52–310	0.54	0.22	[25]

MoS_2/PANI@g-C_3N_4/GCE	4.6–103	9.8–104	0.04	0.062	[26]
MoS_2/PANI/f-MWCNTs/GCE	3.6–125	5.3–125	0.021	0.051	[27]
GR/GCE	3.3–210	2.6–100	0.5	0.3	[28]
O-chit/PPy/WS_2	65.7–2629	51.5–2059	2.83	2.63	[29]
C-chit/PPy/WS_2	65.7–2629	51.5–2059	4.01	3.04	[29]
GQDs@Nafion-AuNPs/ SPCE	0.66–33.0	–	0.32	–	[49]
CuS–H/GCE	0.1–46.5	–	0.053	–	[50]
MWCNTs/GCE	0.01–1.0	–	0.008	–	[51]
PGA/f-MWCNTs/CPE	0.50–18.0	–	0.0199	–	[52]
ZnO/GO-PFA/GrE	–	5.0-155	–	0.15	[53]
GO-RG/CPE	–	8-800	–	0.153	[54]
CNF-GCE	–	25–450	–	17.40	[55]
PPy/Ag-AuBMNPs/PtE	–	0-59	–	2.02	[56]
Nafion-EDA-MWCNTs/BDDE	0.4–40	–	0.12	–	This work
Nafion-EDA-MWCNTs/BDDE	–	0.4–80	–	0.17	This work
Nafion-EDA-MWCNTs/BDDE	0.4–40	0.4–40	0.15	0.18	This work

Abbreviations: AgAuBMNPs: Ag−Au bimetallic nanoparticles, APT-BDDE: Anodically pretreated boron-doped diamond electrode, C-chit: Cicada-chitin, CNFs: carbon nanofibers, CPE: Carbon paste electrode, CPT: Cathodically pretreated, CuS–H: CuS-hexagonal, g-C_3N_4: Graphitic carbon nitride, GCE: Glassy carbon electrode, GO: graphene oxide, GQD: Graphene quantum dots, GrE: Graphite electrode, NGR–NCNTs: Nitrogen-doped graphene/carbon nanotubes, O-chit: Oyster chitin, PANI: Polyaniline, PFA: Phenol formaldehyde amine, Poly(ARS): Poly(alizarin red S), PPy: Polypyrrole, PtE: platinum electrode, RG: Reduced glutathione, SPCE: Screen-printed carbon electrode.

All the parameters demonstrated that the Nafion-EDA-MWCNTs modified BDDE displayed a wider linear detection range or lower sensing limit than the others [23–29,49,52,53,55,56] It has been observed that Nafion-EDA-MWCNTs modified BDDE has exhibited a surpassing electrochemical behavior compared with the reported electrodes from publications (modified or unmodified). Consequently, the Nafion-EDA-MWCNTs modified BDDE was a forceful voltammetric sensor for individual and simultaneous sensing VAN and CAF.

3.8. Selectivity of the method

To study the anti-interference performance of the sensor in this system, several possible interferences of other compounds were detected by SWV. The experimental findings exhibited that the addition of 200 folds of inorganic salts ($CaCl_2$, $MgCl_2$, NaCl, $ZnSO_4$, $CuSO_4$, $Al_2(SO_4)_3$), 100 folds of glucose, ascorbic acid, resorcinol, and phenol and 10 folds of theophylline and theobromine did not influence sensing VAN and CAF (the RSD of the response less than 5%).

3.9. Repeatability, reproducibility, and stability

The repeatability of the constructed Nafion-EDA-MWCNTs/BDDEs was examined by using the same modified BDDE to estimate 10 μM VAN and 10 μM CAF for 5 times. As a result, relative standard

deviations (RSD) of 3.9% and 4.0% were obtained for VAN and CAF, respectively, over five successive determinations. This ideal repeatability could be due to the antifouling features of the Nafion-EDA-MWCNTs/BDDE, which obstruct it from surface fouling. Furthermore, the reproducibility of the modified BDDE was estimated by detecting for 10 µM VAN and 10 µM CAF. In this context, five independent Nafion-EDA-MWCNTs/BDDEs were carefully fabricated in the same fabrication condition and then employed for estimation of VAN and CAF, the experimental results indicate that the invented BDDE-based sensor possesses enough repeatability with RSDs of 3.7% for VAN and 4.4% for CAF. Additionally, the stability of Nafion-EDA-MWCNTs/BDDEs was examined by comparing the oxidation peak current of the invented sensor after storage at 4°C for 15 days. Daily measuring the SWV of VAN and CAF confirmed the stability of the developed modified electrode, the electrode retained 96.4% of its initial oxidation response values after storage. These results confirm that the as-prepared Nafion-EDA-MWCNTs/BDDEs have good stability.

3.10. Application

To confirm the practical applicability of Nafion-EDA-MWCNTs/BDDE in different food samples, a standard addition protocol was applied to determine the concentration of two targets in actual samples. The recovery values were 94-102% and 95-100%, respectively. The RSD of three parallel detections was below 5% (Table 2). The invented sensor displayed relatively good analytical performance for the simultaneous quantification of two analytes in actual samples.

Table 2. Results of the analysis of VAN and CAF content in different food products by using Nafion-EDA-MWCNTs/BDDE.

Sample	Added (mg/L)		Found (mg/L)		Declared (mg/L)		Recovery (%)	
	VAN	CAF	VAN	CAF	VAN	CAF	VAN	CAF
Vanilla sugar	-	-	148.7±1.4	-	150	-	-	-
	30	40	177.6±1.8	38.8±1.2			96	97
	40	50	186.4±2.0	49.2±0.2			94	98
	05	65	198.3±0.9	65.1±0.8			99	100
Energy drink	-	-	-	151.2±1.1	-	150	-	-
	30	40	30.4±0.2	189.3±1.3			101	95
	40	50	39.2±0.5	201.4±1.7			98	100
	50	65	51.1±0.8	216.1±0.9			102	100
Ice Tea	-	-	-	88.2±1.7	-	90	-	-
	30	40	29.6±0.5	128.1±0.6			98	99
	40	50	38.8±1.2	136.8±1.3			97	97
	50	65	48.3±1.8	152.4±1.6			96	98
Vanilla Coffe	-	-	30.4±0.5	298.4±1.8	-	300	-	-
	30	40	58.7±0.5	337.5±0.6			94	97
	40	50	69.4±1.2	346.8±1.3			97	96
	50	65	78.3±1.8	362.4±1.6			95	98

4. CONCLUSIONS

For the first time to our knowledge, an array of BDDEs modified with Nafion-EDA-MWCNTs was fabricated and used in a voltammetric measurement configuration for the simultaneous sensing of VAN and CAF. The Nafion-EDA-MWCNTs materials offer significant improvements in several important figures of merit including linear dynamic range, the limit of detection, response precision and response stability. The invented sensor has displayed resplendent electrochemical responses toward VAN and CAF oxidation at very small concentrations and it has a suitable wide linear range and a low detection limit with convincing repeatability, selectivity and stability. In addition, the proposed approach has been successfully utilized for the quantification of VAN and CAF in actual samples, which shows that the EDA-MWCNT-based electrochemical sensor is convenient for use in food analysis and food safety. Furthermore, Nafion-EDA-MWCNTs/BDDE could be employed for the multi-component analysis in food control and the chemical industry.

ACKNOWLEDGEMENTS
The authors gratefully acknowledge the use of the facilities of Istanbul University-Cerrahpaşa (Istanbul/Turkey).

AUTHOR CONTRIBUTION:
Babak Hatami Baroogh: Performed the measurements, processed the experimental data, performed the analysis, and designed the figures. Asiye Aslıhan Avan: Performed the measurements, processed the experimental data, performed the analysis, and designed the figures. Hayati Filik: Drafted the manuscript and was involved in planning and supervising the work, aided in interpreting, the results and worked on the manuscript. Sibel Yalçın: Processed the experimental data. All authors discussed the results and commented on the manuscript.

FUNDING:
No funding was received for this study.

DATA AVAILABILITY:
The dataset analyzed during the current study is available from the corresponding author upon reasonable request.

DECLARATIONS

ETHICS APPROVAL:
This article does not contain any studies with human participants or animals performed by any of the authors.

INFORMED CONSENT:
Informed consent is not applicable.

CONFLICT OF INTEREST:
The authors declare no competing interests

References

1. G. Banerjee, P. Chattopadhyay, *J. Sci. Food Agric.*, 99 (2019) 499–506.
2. G.A. Martău, L.F. Călinoiu, D.C. Vodnar, *Trends Food Sci. Technol.*, 109 (2021) 579–592.
3. S.S. Arya, J.E. Rookes, D.M. Cahill, S.K. Lenka, *Adv. Tradit. Med.*, 21 (2021) 1–17.
4. V. Paul, D.C. Rai, R.L. Ramyaa, S.K. Srivastava, A.D. Tripathi, *Food Biotechnol.*, 35 (2021) 22–49.
5. T.M. McLellan, J.A. Caldwell, H.R. Lieberman, *Neurosci. Biobehav. Rev.*, 71 (2016) 294–312.
6. C. Willson, *Toxicol. Reports*, 5 (2018) 1140–1152.
7. D. Wikoff, B.T. Welsh, R. Henderson, G.P. Brorby, J. Britt, E. Myers, J. Goldberger, H.R. Lieberman, C. O'Brien, J. Peck, M. Tenenbein, C. Weaver, S. Harvey, J. Urban, C. Doepker, *Food Chem. Toxicol.*, 109 (2017) 585–648.
8. A.C. Alves, A.D. Meinhart, J. Teixeira Filho, H.T. Godoy, *Food Sci. Technol.*, 39 (2019) 673–682.
9. A. Ahmed Elbashir, R. Elamin Elgack Elgorashe, A.O. Alnajjar, H.Y. Aboul-Enein, P.Y. Hassan Aboul-Enein, P.A. Abdalla Elbashir, *Sep. Sci. Plus*, 4 (2021) 266–272.
10. Y. Ni, G. Zhang, S. Kokot, *Food Chem.*, 89 (2005) 465–473.
11. C. Raril, J.G. Manjunatha, *Microchem. J.*, 154 (2020) 104575.
12. A.B. Monnappa, J.G.G. Manjunatha, A.S. Bhatt, H. Nagarajappa, *J. Sci. Adv. Mater. Devices*, 6 (2021) 415–424.
13. V. Erady, R.J. Mascarenhas, A.K. Satpati, *Sensors Int.*, 1 (2020) 100023.
14. P.A. Pushpanjali, J.G. Manjunatha, G. Tigari, S. Fattepur, *Anal. Bioanal. Electrochem.*, 12 (2020) 553–568.
15. L. Fu, K. Xie, D. Wu, A. Wang, H. Zhang, Z. Ji, *Mater. Chem. Phys.*, 242 (2020) 122462.
16. T. Tabanlıgil Calam, *Food Chem.*, 328 (2020) 127098.
17. O. Sarakhman, A. Benková, Ľ. Švorc, *Microchem. J.*, 175 (2022) 107132.
18. P.C.G. Júnior, V.B. dos Santos, A.S. Lopes, J.P.I. de Souza, J.R.S. Pina, G.C.A. Chagas Júnior, P.S.B. Marinho, *Food Control*, 108 (2020) 106887.
19. R. Hallaj, E. Soltani, S. Mafakheri, M. Ghadermazi, *Mater. Sci. Eng. B*, 274 (2021) 115473.
20. N.A. Nia, M.M. Foroughi, S. Jahani, *Talanta*, 222 (2021) 121563.
21. A. Wong, A.M. Santos, R. da Fonseca Alves, F.C. Vicentini, O. Fatibello-Filho, M. Del Pilar Taboada Sotomayor, *Talanta*, 222 (2021) 121539.
22. L. Jiang, Y. Ding, F. Jiang, L. Li, F. Mo, *Anal. Chim. Acta*, 833 (2014) 22–28.
23. H. Filik, A.A. Avan, Y. Mümin, *Food Anal. Methods*, 10 (2017) 31–40.
24. H.S. Ali, A.A. Abdullah, P.T. Pınar, Y. Yardım, Z. Şentürk, *Talanta*, 170 (2017) 384–391.
25. N. Alpar, Y. Yardım, Z. Şentürk, *Sensors Actuators B Chem.*, 257 (2018) 398–408.
26. E. Murugan, A. Dhamodharan, *Diam. Relat. Mater.*, 120 (2021) 108684.
27. E. Murugan, A. Dhamodharan, *Diam. Relat. Mater.*, 128 (2022) 109268.
28. A. Yiğit, N. Alpar, Y. Yardım, M. Çelebi, Z. Şentürk, *Electroanalysis*, 30 (2018) 2011–2020.
29. S. Selvam, J.H. Yim, *J. Energy Storage*, 45 (2022) 103791.
30. S. Baluchová, A. Daňhel, H. Dejmková, V. Ostatná, M. Fojta, K. Schwarzová-Pecková, *Anal. Chim. Acta*, 1077 (2019) 30–66.
31. K. Muzyka, J. Sun, T.H. Fereja, Y. Lan, W. Zhang, G. Xu, *Anal. Methods*, 11 (2019) 397–414.
32. T. Kondo, *Curr. Opin. Electrochem.*, 32 (2022) 100891.
33. Y. Yardim, E. Keskin, Z. Şentürk, *Talanta*, 116 (2013) 1010–1017.
34. P. Niedziałkowski, R. Bogdanowicz, P. Zieba, J. Wysocka, J. Ryl, M. Sobaszek, T. Ossowski, *Electroanalysis*, 28 (2016) 211–221.
35. B.C. Lourenção, R.A. Medeiros, R.C. Rocha-Filho, O. Fatibello-Filhoa, *Electroanalysis*, 22 (2010) 1717–1723.
36. R. Bansal, R. Verduzco, M.S. Wong, P. Westerhoff, S. Garcia-Segura, *J. Electroanal. Chem.*,

907 (2022) 116028.
37. P. Gan, J.S. Foord, R.G. Compton, *ChemistryOpen*, 4 (2015) 606–612.
38. H. Filik, A.A. Avan, N. Altaş Puntar, M. Özyürek, Z.B. Güngör, M. Kucur, H. Kamış, D.A. Dicle, *J. Electroanal. Chem.*, 900 (2021) 115700.
39. Z. Zang, Z. Hu, Z. Li, Q. He, X. Chang, *J. Hazard. Mater.*, 172 (2009) 958–963.
40. K. Lee, J.W. Lee, S. Il Kim, B.K. Ju, *Carbon N. Y.*, 49 (2011) 787–792.
41. E. Laviron, *J. Electroanal. Chem. Interfacial Electrochem.*, 101 (1979) 19–28.
42. F.C. Anson, Y.M. Tsou, J.M. Savéant, *J. Electroanal. Chem. Interfacial Electrochem.*, 178 (1984) 113–127.
43. C.F. Shu, F.C. Anson, *J. Am. Chem. Soc.*, 112 (1990) 9227–9232.
44. E. Sabatani, H.D. Nikol, H.B. Gray, F.C. Anson, *J. Am. Chem. Soc.*, 118 (1996) 1158–1163.
45. Y.X. Chen, S. Ye, M. Heinen, Z. Jusys, M. Osawa, R.J. Behm, *J. Phys. Chem. B*, 110 (2006) 9534–9544.
46. T. Ramanathan, F.T. Fisher, R.S. Ruoff, L.C. Brinson, *Chem. Mater.*, 17 (2005) 1290–1295.
47. U.J. Kim, C.A. Furtado, X. Liu, G. Chen, P.C. Eklund, *J. Am. Chem. Soc.*, 127 (2005) 15437–15445.
48. J.C. Miller, J.N. Miller, Statistics for Analytical Chemistry, 4rd ed., Ellis Horwood PTR Prentice Hall, (1993) New York.
49. G.M. Durán, E.J. Llorent-Martínez, A.M. Contento, Á. Ríos, *Microchim. Acta*, 185 (2018) 204.
50. S. Radhakrishnan, J. Mathiyarasu, B.S. Kim, *Appl. Mater. Today*, 27 (2022) 101428.
51. I. Kouhi, G. Parvizi Fard, E. Alipour, A. Saadatirad, *J. Food Process. Preserv.*, 46 (2022) e16289.
52. N. Hareesha, J.G. Manjunatha, B.M. Amrutha, N. Sreeharsha, S.M. Basheeruddin Asdaq, M.K. Anwer, *Colloids Surfaces A Physicochem. Eng. Asp.*, 626 (2021) 127042.
53. A.M. Madhusudhana, K.N.S. Mohana, M.B. Hegde, N.K. Swamy, S.A. Shivamurthy, *Diam. Relat. Mater.*, 130 (2022) 109531.
54. M. Shehata, S.M. Azab, A.M. Fekry, *Synth. Met.*, 256 (2019) 116122.
55. T.I. Sebokolodi, D.S. Sipuka, T.R. Tsekeli, D. Nkosi, O.A. Arotiba, *J. Food Meas. Charact.*, 16 (2022) 2536–2544.
56. K.K. Masibi, O.E. Fayemi, A.S. Adekunle, E.S.M. Sherif, E.E. Ebenso, *Electroanalysis*, 32 (2020) 2745–2755.